

Looking Twice for Partial Clues: Weakly-supervised Part-Mentored Attention Network for Vehicle Re-Identification

Lisha Tang, Yi Wang, *Member, IEEE*, Lap-Pui Chau, *Fellow, IEEE*

Abstract—Vehicle re-identification (Re-ID) is to retrieve images of the same vehicle across different cameras. Two key challenges lie in the subtle inter-instance discrepancy caused by near-duplicate identities and the large intra-instance variance caused by different views. Since the holistic appearance suffers from viewpoint variation and distortion, part-level feature learning has been introduced to enhance vehicle description. However, existing approaches to localize and amplify significant parts often fail to handle spatial misalignment as well as occlusion and require expensive annotations. In this paper, we propose a weakly-supervised Part-Mentored Attention Network (PMANet) consisting of a Part Attention Network (PANet) for vehicle part localization with self-attention and a Part-Mentored Network (PMNet) for mentoring the global and local feature aggregation. Firstly, PANet is introduced to predict a foreground mask and pinpoint K prominent vehicle parts only with a weak identity supervision. Secondly, we propose a PMNet to learn global and part-level features with multi-scale spatial and channel attention and aggregate them in K main-partial tasks via part transfer. Like humans who first differentiate objects with general information and then observe salient parts for more detailed clues, PANet and PMNet construct a two-stage attention structure to perform a coarse-to-fine search among identities. Finally, we address this Re-ID issue as a multi-task problem, including global feature learning, identity classification, and part transfer. We adopt Homoscedastic Uncertainty to learn the optimal weighing of different losses. Comprehensive experiments are conducted on two benchmark datasets. Our approach outperforms recent state-of-the-art methods by averagely 2.63% in CMC@1 on VehicleID and 2.2% in mAP on VeRi776. Moreover, Experimental results on occluded test sets demonstrate that PMANet has a good generalization ability.

Index Terms—Vehicle re-identification, weak supervision, part attention, multi-task learning.

I. INTRODUCTION

Given a query vehicle image, vehicle re-identification (Re-ID) aims at identifying all images with the same identity in a gallery set across multiple non-overlapping cameras. It holds great potential in public security as well as intelligent transportation, thereby drawing increasing attention from both academia and industry. Despite this, various challenges still hinder the performance of vehicle Re-ID (see Fig.1(a)): (1) the viewpoint variation problem: a vehicle viewed in different camera orientations usually exhibit dramatically different visual appearances; (2) near-duplicated phenomenon [2]:

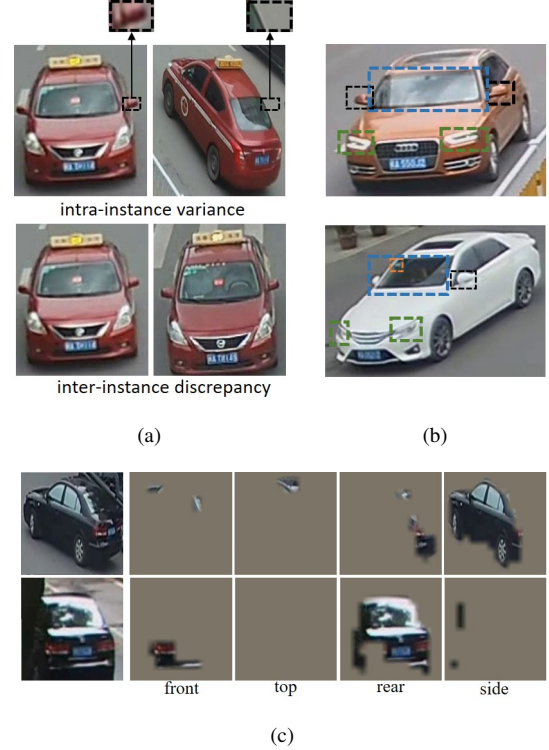


Fig. 1. (a) The two images in the first row show the dramatic variance in visual appearance of the same vehicle caused by viewpoint changes, while the images in the second row illustrate the minor inter-instance discrepancy caused by near-duplicate challenge. Furthermore, the two zoomed-in patches show that the same spatial position across two images may not correspond to the same vehicle part. (b) The orange, green, blue and black rectangles respectively show different vehicle components: annual labels, headlights, windscreen, and side-view mirrors. Apparently, they exhibit large scale and shape variation. (c) The figures show the four view-aware masks of two sample images generated by PVEN [1].

different vehicles with the same type and color may look quite similar especially when the images are captured from one single unified view. The former increases intra-instance variance, while the latter decreases inter-instance discrepancy. Previous works that only rely on global information [3], [4] are proved ineffective because holistic features are often sensitive to interference, such as viewpoint variation, illumination changes, and background clutter and fail to supply fine-grained cues.

Recent works elaborately aggregated local features with global ones to provide complementary information. For example, [5], [6] extract local features based on three vertically

Lisha Tang, Yi Wang, and Lap-Pui Chau are with School of Electrical and Electronic Engineering, Nanyang Technological University, Singapore, 639798 (e-mail: lisha001@e.ntu.edu.sg, wang1241@e.ntu.edu.sg, elpchau@ntu.edu.sg). Corresponding author: Lap-Pui Chau.

separated vehicle regions to acquire distinctive visual cues. However, as shown in the first row of Fig.1(a), such naive uniform division fails to handle spatial component misalignment because the same spatial position across two images may not correspond to the same vehicle part. Particularly, in cases where a car body is not evenly distributed in the image, uniform division might miss some crucial information due to such misalignment. Other methods also pre-define regions or parse an image into view-aware parts to shrink intra-instance discrepancy [1], [2], [6], [7], [8], [9], [10], [11]. Among them, He *et al.* [2] pre-defined windows, lights and brands for each vehicle and used them to train a YOLO [12] detector. PVEN [1] labels 20 key-points of each vehicle and parses each image into four views based on them. Nevertheless, these methods require substantial part-level annotations, which are labor-intensive. Hence, it is still challenging to locate informative vehicle parts without extra annotations. Moreover, as regards joint learning of global and local features, existing standard local feature learning methods [13], [2], [8], [1], [7] simply use convolutional or fully connected layers in a single local branch to extract a part-specific feature, which poses two weaknesses. Firstly, it requires vehicle part masks for both training and testing. Secondly, such a structure only learns part-level features within each part mask. However, these masks from existing methods are not always accurate (see Fig.1(c)), thus introducing noises during testing.

To tackle the aforementioned challenges, this paper proposes a Part-Mentored Attention Network (PMANet) to achieve weakly-supervised vehicle part localization and part-mentored global-local feature alignment for vehicle Re-ID, as shown in Fig.2. Specifically, our PMANet consists of two steps: a weakly-supervised Part Attention Network (PANet) and a Part-Mentored Network (PMNet). When distinguishing different objects, humans first leverage some obvious general information, such as color, shape and vehicle component segments (e.g., windscreens, headlights). Then for near-duplicate cases, our eyes zoom in these informative components and observe them closely to mine more detailed clues. To mimic such a coarse-to-fine recognition strategy, we construct a two-stage hard-soft attention mechanism within the two steps. Firstly, PANet predicts a refined foreground mask and robustly locates K prominent vehicle parts to address spatial misalignment and background interference. PANet learns a part-aware localization facility under weak supervision by modeling the inter-channel relationships of the encoded feature map and applies a hard self-attention for K partial mask prediction via a Trilinear Attention Module and a Part Mask Generation Module. Secondly in PMNet, we build a backbone network followed by two head networks, i.e., Global Feature Learning Head (GFLH) and Part-Mentored Learning Head (PMLH). With the K part masks from PANet, PMLH is composed of K branches which respectively focus on K different vehicle parts. To handle the two weaknesses of the standard single local branch structure, we do not totally trust part masks. The proposed branch instead builds one Main Task and one Partial Task, focusing on the global feature space and one vehicle part feature space, respectively. Each Partial Task is regarded as a noisy teacher and guides its student, the correspondent Main

Task, to concentrate on the same vehicle part. Such guidance between each Main-Partial Task pair is realized by a novel part transfer constraint. To conduct a second closer look at the details within each vehicle part, a soft Multi-scale Attention Module (MAM) is introduced into each Main-Partial Task.

Moreover, we model this Re-ID issue as four sub-tasks, including global feature learning, identity classification for global features, identification classification for part features, and part transfer for Main-Partial Task pairs under a shared backbone. These four sub-tasks compensate and facilitate each other, thus improving the model generalization and performance. Besides, Homoscedastic Uncertainty Learning [14] is adopted to help speed the convergence process during training and learn loss weighting without manual tuning. Overall, the proposed method is evaluated on two public vehicle Re-ID datasets, including VeRi776 [3] and VehicleID [15]. Experiments and ablation analysis demonstrate that our method yields superior performance over state-of-the-art models. Results on occluded test sets also prove that our method effectively resists the obstruction in the occluded vehicle images.

The remainder of the paper is organized as follows. Related works are briefly reviewed in Section II and the detailed model structure is described in Section III. Afterwards, Section IV presents implementation details and experiments, followed by the conclusion in Section V.

II. RELATED WORK

A. Vehicle Re-ID

Derived from person Re-ID, vehicle Re-ID has attracted increasing attention, but the performance is far from satisfactory. As one of the pioneer works to study vision-based vehicle re-ID model, [3] combines hand-crafted features like SIFT and Color Name with deep features extracted from CNN models. With recent breakthroughs of deep learning, experiments demonstrate that deep features are more discriminative than hand-crafted ones. Since then, many deep models have been introduced to push the boundaries of vehicle Re-ID.

1) *Attribute-based feature learning*: Early deep learning methods directly incorporated various meta information such as vehicle attributes (e.g., model, color) and spatial-temporal information to enhance global feature representation. [16] fuses camera views, vehicle types and color into feature embedding. [4] reduces searching space by utilizing visual-spatial-temporal paths. However, these global representation-based approaches suffer from the instability caused by dramatic viewpoint changes and challenges brought by the large intra-class variance. Besides, attributes and spatial-temporal cues are not always available, limiting the application of those algorithms. In contrast, our work does not consider the usage of additional information or annotations.

2) *Regional feature learning*: To learn more discriminative details that holistic features fail to provide, recent works take local feature learning into account. Current regional feature learning methods can be grouped into three categories. The first category [6], [5], [17] utilizes uniform division, which vertically splits the image or feature map into several regions

of equal area. However, as is mentioned in the Introduction, such naive division suffers from spatial component misalignment. Others [2], [6], [7], [8], [1], [9], [10], [11] pre-define vehicle components for subtle local cues. Zhao *et al.* [9] collected a vehicle dataset with 21 classes of attribute labels and trained the Single-Shot Detector [18]. He *et al.* [2] detected windows, lights, and brands for each vehicle through a YOLO [12] detector to generate discriminative features. The third type learns viewpoint-specific features. For example, SPAN [8] predicts part attention masks for different views and emphasizes co-occurrence parts when computing the feature distances. MVAN [19] proposes a multi-view branch network, where each branch focuses on a limited range of viewpoint changes. However, all the methods above require additional data annotations. Besides, TAMR [7] leverages two STNs [20] to locate windcreens and car heads, and constrains its model with a Multi-Grain Ranking loss. Apart from requiring central coordinates of these two vehicle components, TAMR also ignores other vehicle parts, which might also contain important local information (e.g., front bumper, tires). It is also notable that headlights and windscreen cannot be captured under some views, such as side view. Therefore, self-supervised and weakly-supervised vehicle part localization is still challenging.

Some other localization methods, e.g., SCDA [21], PL-Net [22] and PAN [23], are proposed based on the principle that different channel groups tend to exhibit strong activation on regions with different semantic meanings. PAN [23] relocates the pedestrian with STN [20] and merges it with the feature of the original image to form a new pedestrian descriptor. However, this method merely concentrates on re-localization of the full human body but fails to take advantage of the fine-grained details which can be provided by different body parts. PL-Net [22], which clusters the coordinates with the maximum response of each channel for component localization, is proved quite unstable because without further channel grouping, feature maps of the encoder are sensitive to inference (e.g., noises and background clutter), and pixels with the maximum response might be noise or lie in the same body part of a person. Differently, our method can perform vehicle part localization robustly.

3) *Other vehicle Re-ID methods:* Some researchers also design models based on Long Short-Term Memory (LSTM) and Generative Adversarial Networks (GAN) in vehicle Re-ID. For instance, Zhou *et al.* [24] exploited the great advantages of the LSTM to model transformations across continuous view variations of a vehicle. Lou *et al.* [25] proposed a GAN-based model for hard sample generation. Nevertheless, due to the limitation of generation ability of existing GAN and the insufficient adversarial samples, there still exists a large gap between the generated samples and real ones. In addition, transfer learning is recently introduced to person Re-ID [26], [27], [28]. A DSAG-Stream designed in [26] acts as a regulator to guide an MF-Stream for densely semantically aligned feature learning. [28] handles body part misalignment via multi-task learning in a student-teacher manner. However, relevant exploration in vehicle Re-ID is quite insufficient. Inspired by [28], our PMNet aligns global and local features in part concept transfer manner to enlarge inter-instance discrepancy

especially between similar cases.

B. Occluded Re-ID

Different from traditional Re-ID task which performs pedestrian or vehicle retrieval in the full-body domain, occluded Re-ID is a challenging practical issue since occlusion generally occurs in real-world scenarios. Currently occluded person Re-ID has attracted much attention but there is still little research related to occluded vehicle Re-ID. [29] increases the model generalization by synthesizing occlusion samples and resorts to an attention mechanism for fine-grained feature learning. ASAN [30] proposes a CAM-based segmentation module and a shift feature adaptation module to extract features within the visible part of the image. It designs an occluded test set based on VeRi776 [3], and conduct comparison experiments on it. However, this method uses vehicle model and color information which are not always available.

C. Attention Mechanism

Attention mechanism in deep learning, which mimics the human visual attention mechanism [31], has been adopted in many vision tasks to mine more discriminative information. The matrix multiplication in self-attention draws global dependencies of each word in a sentence [32] or each pixel in an image [33]. SE-Net [34] squeezes global spatial information into a channel descriptor to capture channel-wise dependencies. All these methods concentrate on a global scale. Recently, researchers have realized that the scale variation of objects plays a vital role in many fine-grained tasks (see Fig.1(b)) and introduced multi-scale attention to handle such issue in CNNs. Previous works usually use classic convolutional filters with multiple kernel sizes (e.g., 3×3 , 5×5 , 7×7), which overlap with each other at the same output position and thereby causes much redundant information. In contrast, we employ convolutional layers of multiple dilation ratios to learn multi-scale features.

Recent vehicle Re-ID works also introduce attention modules [35], [10], [7], [19]. Among them, Teng *et al.* [35] proposed a spatial and channel attention network to refine feature maps in the two dimensions. Teng *et al.* [10] proposed a channel-wise Part Attention Module to indicate the importance of each part feature. Nevertheless, research in multi-scale attention is still limited and all these methods employ attention either for detailed part clues or for weighting of their extracted features. In this paper, we construct a two-stage hard-soft attention structure which performs a second look at the refined region to mine features of multiple granularities.

III. METHODOLOGY

When differentiating objects, humans first utilize obvious general information for easy samples, then observe salient components closely for more discriminative clues to distinguish near-identical cases. Our method mimics such human strategy and performs a coarse-to-fine search on vehicles. As illustrated in Fig.2, our proposed model consists of two steps: a weakly-supervised Part-Attention Network (PANet) in

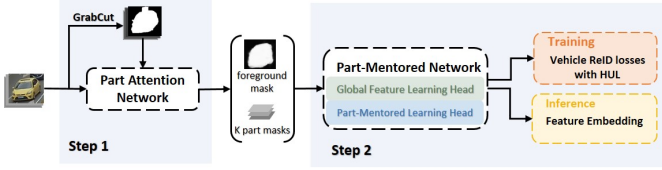


Fig. 2. Pipeline of our method. Our proposed method consists of two steps, Part Attention network (PANet) and Part-Mentored Network (PMNet). Utilizing coarse masks by GrabCut [36] as pseudo labels, PANet refines the foreground mask and predicts K part masks without part-level supervision. They are fed into PMNet for global and local feature learning.

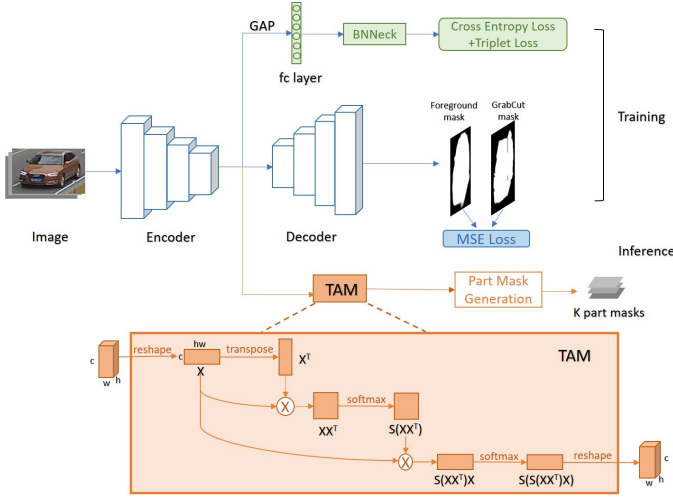


Fig. 3. Architecture of the Part Attention Network. As the blue arrow lines show, during training, the PANet combines a classic Re-ID baseline model [37] and an encoder-decoder style segmentation model to learn discriminative features for identity classification and reconstruct a foreground mask at the same time. The orange arrow lines illustrate the pipeline to predict K part masks in the inference stage and details of the Trilinear Attention Module (TAM) are shown in the orange rectangle. $S(\cdot)$ in TAM indicates softmax normalization and \otimes denotes matrix multiplication.

Sec.III-A and a Part-Mentored Network (PMNet) in Sec.III-B. In Sec.III-C, we model the entire Re-ID issue as four sub-tasks and incorporate Homoscedastic Uncertainty Learning to automatically balance the joint learning of the ID losses.

A. Part Attention Network for Vehicle Part Localization

To handle the misalignment problem caused by viewpoint and position variations, Part Attention Network (PANet) aims at predicting a refined foreground mask and automatically locating K part masks which focus on different vehicle parts. In addition to avoiding background interference, these masks help derive a more comprehensive and reliable representation of the vehicle in step 2. Experiments in Sec.IV-E also demonstrate the robustness to occlusion. Specifically, we first generate coarse foreground masks of vehicles using the handcrafted segmentation algorithm, GrabCut [36]. However, these masks are unstable and often contain errors, thereby are used as pseudo labels for PANet.

Inspired by [38], PANet combines a classic classification and segmentation model in a unified framework to extract discriminative features for identity classification and foreground mask refinement, as shown in Fig.3. Our PANet employs

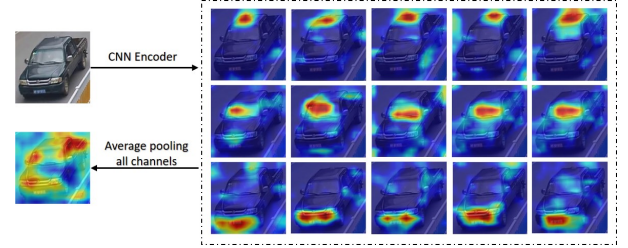


Fig. 4. Examples of attention maps of the output feature channels generated by the CNN encoder. The two figures on the left are the input vehicle image and the attention map after average pooling all the channels. The figures on the right are respectively attention visualizations of channels which indicate different vehicle parts, e.g., vehicle roof, windcreens and head lights. The images on each row exhibit channels that fire on the same region.

ResNet-50 [39] as the feature encoder. In the classification branch, the feature map from the encoder is fed into a fully connected layer, a BNNeck [37] to compute ID loss and triplet loss [40]. In the segmentation branch, four blocks are introduced as the decoder to calculate the Maximum Squared Error (MSE) loss between its reconstructed masks and coarse pseudo masks. In specific, the first three blocks are composed of one transposed convolutional layer, a batchnorm and ReLU layer, while the last one consists of a transposed convolutional layer and Sigmoid. The segmentation branch considers vehicle structure to help inform class boundary decisions, while the classification branch introduces instance-specific supervision and helps weigh the importance of different vehicle parts. Such a combination of the classic classification as well as segmentation framework leads to a compromise between the classification task and the segmentation task under the same backbone. During inference, PANet generates a refined foreground mask and the feature maps of the encoder. The feature maps are further fed into a Trilinear Attention Module (TAM) and Part Mask Generation module to predict K part attention masks.

1) *Trilinear Attention Module*: Recent works in Person Re-ID have shown that different channel groups of the feature map for a person activate local responses at their corresponding body parts [22]. Similar correspondences between channels and vehicle parts are also observed in vehicle Re-ID. As depicted in Fig.4, although information conveyed by each single channel is weak and sensitive, many channels usually tend to activate on the same region which may indicate different semantically meaningful parts (e.g., car roof, windcreens, and headlights). This property can assist in locating different vehicle parts in the spatial dimension, thereby learning detailed local information within each vehicle part. However, some channels might be sensitive to noise and activate at the background or other wrong spots, creating a negative impact on the overall performance (e.g., PL-Net [22]). Therefore, it is important to design a network which helps accurately group different channels and suppress noise. With this goal, we propose a Trilinear Attention Module to convert the feature map to a more robust and consistent attention map, and then the map is fed into a Part Mask Generation module to locate partial masks.

As Fig.3 depicts, during inference, given an input image,

we obtain the feature map from the encoder with a dimension of $C \times H \times W$, where C , H and W respectively indicate the channel number, height, and width. After reshaping the feature map into a matrix, $X \in \mathbb{R}^{C \times HW}$, we compute the bilinear feature, $G(X) = \text{softmax}(X \cdot X^T)$, which indicates the relationship between the channels.

Since channels within a channel group concentrate on the same part, $G(X)$ can group the channels of the feature map with a bilinear product and the *softmax* operation employed here computes the similarity between any two channels. The larger $G_{i,j}(X)$ is, the more similar channel i and channel j are, i.e., the more likely channel i and channel j concentrate on the same vehicle part. Then, we get a more consistent feature map by multiplying $G(X)$ with the reshaped feature map, X . In this way, for each channel, important information about the vehicle region is amplified by other channels within the same group, while noisy information is reduced. Another *softmax* is conducted on the output feature map to generate a normalized attention map. This trilinear function can be formulated as,

$$F(X) = S(S(X \cdot X^T) \cdot X), \quad (1)$$

where $S(\cdot)$ indicates softmax normalization over the second dimension of the matrix. Finally, the attention map is reshaped to $C \times H \times W$. In brief, this self-trilinear product suppresses influence of background clutter as well as random noise, conducts further channel grouping, and generates a more stable attention map.

2) *Part Mask Generation*: Afterwards, the generated normalized attention maps are fed into the Part Mask Generation module to predict partial masks. In specific, we first obtain the bounding box of the largest connected domain of each channel, calculate the corresponding central coordinate and conduct k-means clustering on all these central coordinates according to their positions in each feature map. K cluster centers are obtained and thus, K rectangular partial masks are gained. Here, for each partial mask, we set the height $h = \frac{H}{K}$; $w = \frac{W}{K}$.

B. Part-Mentored Network for Vehicle Re-ID

In this section, we first introduce the motivation and problem formulation of vehicle Re-ID. Then, the details of our Part-Mentored Network (PMNet), including global feature learning head and the Part-Mentored Learning Head (PMLH), are presented. The overall architecture is depicted in Fig.5.

1) *Problem Formulation for Re-ID*: Given a vehicle query image I_q , vehicle Re-ID aims to retrieve the images with the same identity from a gallery set G . We denote the gallery set as $G = \{I_i\}$, $i \in [1, m]$, where m is the total number of images in the gallery set. This issue is usually tackled by learning a discriminative feature representation f for each image from a training set. Therefore, the retrieval process can be simplified as matching the feature representation of the query, f_q , with those of the gallery images, f_G .

In our paper, we model this Re-ID issue as 4 sub-tasks under a shared backbone, including global feature learning, classification task for the global feature, classification task for

part features, and part transfer between Main-Partial Task pairs (see Sec.III-C). With the shared backbone, these 4 tasks can be jointly trained in our unified feature learning network and achieve the optimal model generalization.

2) *Global Feature Learning Head*: Our part-mentored feature learning network utilizes ResNet-50 as backbone, which is split into two head networks by two separate *res_conv5* residual stages because using a backbone which shares it might dilute the importance of detailed information [41]. Our global feature learning head aims to conduct a coarse look at the entire image and extract apparent global information to distinguish identities with significant appearance differences. To increase the size of the output feature maps, we remove the last spatial down-sampling operation of both *res_conv5*.

As is shown in Fig.5, our global branch feeds the output feature map of the backbone into several convolutional layers, a Global Average Pooling (GAP) and a BNNeck layer [37]. The learning process is supervised by one Triplet loss [40] and one ID loss.

3) *Part-Mentored Learning Head*: Standard regional feature-based methods [13], [2], [8], [1], [7] simply use a single branch for local feature extraction on each vehicle part, but this causes two weaknesses. First, it requires vehicle part masks for both training and inference. Second, it only learns part-level features within each part mask. However, part masks from existing models are not always accurate (see Fig.1(c)). Such inaccurate part masks will introduce noises especially during inference. In our paper, we introduce PMLH to perform a second closer look at the localized vehicle parts for more robust, discriminative partial features and aligns them with the global one in a part transfer manner.

As Fig.5 shows, PMLH is composed of K branches, which respectively concentrate on K vehicle parts localized by the first step, PANet. Each branch utilizes one 1×1 Conv layer to combine relevant channels for the specific vehicle part from the output feature maps of the backbone. After the 1×1 Conv layer, each branch builds two tasks, the Main Task (MT) and the Partial Task (PT), which respectively focuses on the holistic feature space and one vehicle part feature space. All the MTs and PTs are similar in architecture but have different inputs. Specifically, each MT incorporates one Multi-scale Attention Module (MAM), GAP, one BNNeck layer [37] and a classification layer. The GAP in each MT learns translation and scale-invariant holistic feature. Each PT replaces GAP with a Mask Max Pooling (MMP) layer, which can be implemented as a Max Pooling layer with pooling size equal to the area of partial masks. Compared with GAP, MMP helps mine more significant local features within the constrained mask region. To handle the two weaknesses of the standard single local branch structure, we do not totally trust part masks. Instead, to learn more robust local features, each part mask branch, i.e., Partial Task, is regarded as a noisy teacher. During training, the Partial Task guides its student, the correspondent Main Task, to concentrate on the same vehicle part. Such guidance is realized by our proposed sample-wise Part Transfer loss. Since Main Tasks learn features within the entire feature map, F_K , it avoids degrading by the noises from inaccurate vehicle part masks. Moreover, these Partial Tasks

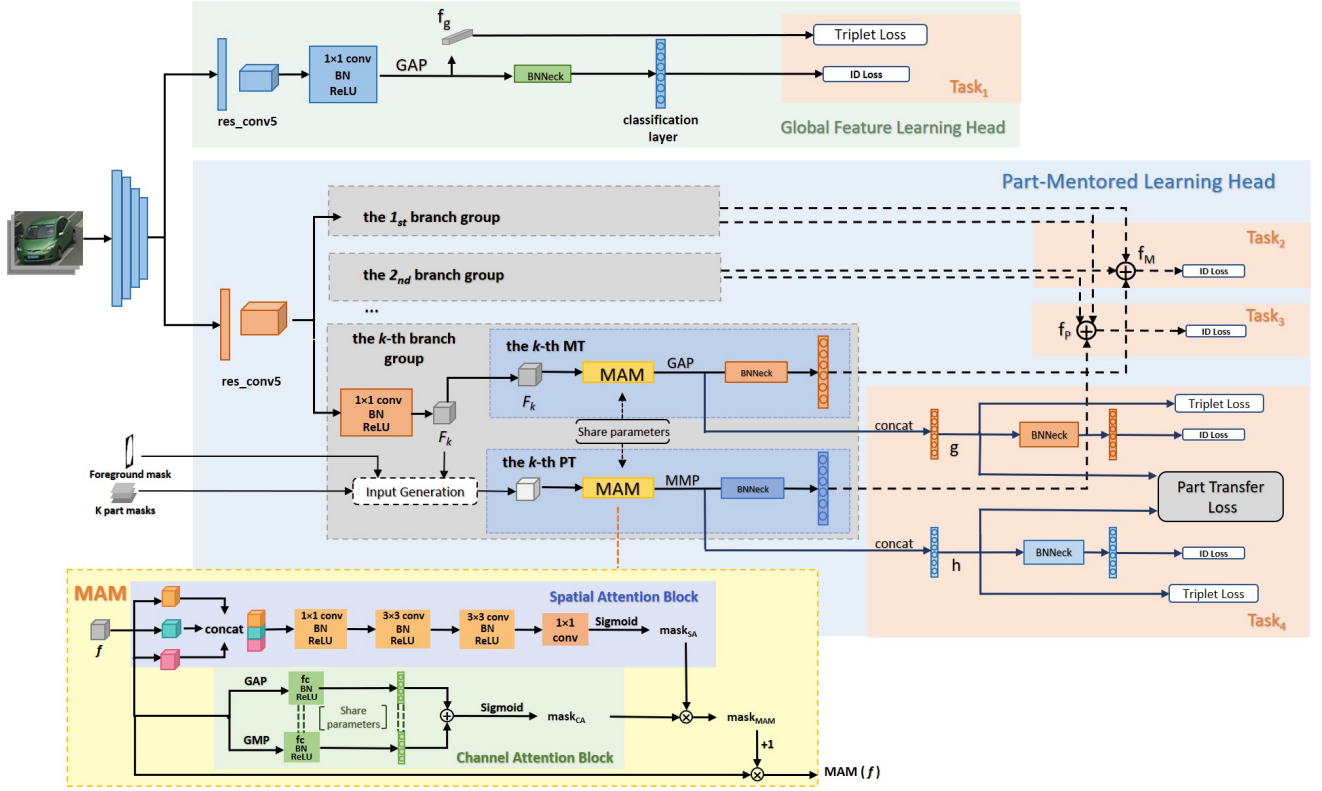


Fig. 5. Architecture of the Part-Mentored Network. The ResNet-50 backbone is split into two sub-networks with two *res_conv5* residual blocks: the Global Feature Learning Head (in green) and the Part-Mentored Learning Head (in blue). As the blue block shows, PMLH is composed of K branches which consists of one Main Task (MT) and one Partial Task (PT). With different inputs, these two tasks are similar in architecture and share one Multi-scale Attention Module (MAM). As shown in the yellow block, MAM utilizes three convolutional layers with multiple dilation ratios to mine multi-scale features in its Spatial Attention Block and obtain a spatial attention mask, $mask_{SA}$. An output channel attention mask, $mask_{CA}$, is generated by Channel Attention Block. Then these two masks are multiplied together to gain $mask_{MAM}$. The orange area respectively illustrate loss functions employed in four sub-tasks. Here \otimes denotes element-wise multiplication and \oplus indicates element-wise summation.

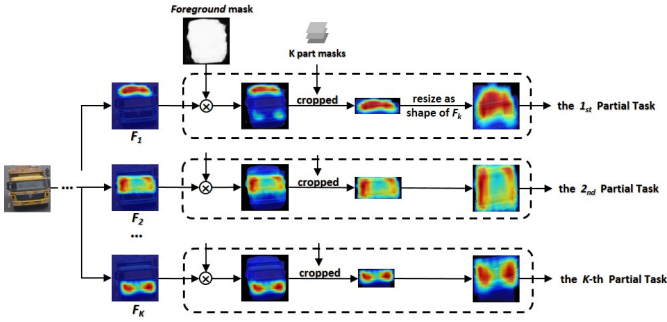


Fig. 6. Input generation for Partial Tasks. The dashed block shows details of the Input Generation module in Fig.5. After being multiplied with the refined foreground mask, the feature map F_K is further cropped according to the K -th bounding boxes of the K -th part mask and then resized to the shape of F_K . Here we set $K = 3$ in our experiment and show visualization maps of the three inputs for Part Tasks. It can be observed that these maps respectively focus on three different parts with semantic meaning, i.e., vehicle roof, windscreen and headlights.

can be removed during inference, which means that our PMNet can also be free from PANet during testing.

The major difference between each MT-PT pair of one vehicle part lies in their inputs. The input of each MT is the original feature map after the 1×1 Conv layer, F_K ,

while each PT is equipped with the correspondent partial feature map during training. As illustrated in Fig.6, we first multiply F_K with the refined foreground mask. Afterwards, the multiplied feature map is separately cropped according to the bounding boxes of the K part masks from PANet. Since each MT and PT are similar in architecture and require the same input size, the cropped feature map is resized as the shape of F_K via bilinear interpolation. In this way, K input feature maps for PTs are obtained. They can provide guidance for MTs to amplify channels relevant to the correspondent vehicle parts via part transfer, which will be detailed presented in Sec.III-B3. During inference, our method achieves state-of-the-art performance without PTs, which means our PMLH can be free from prior mask generation of PANet. Results in Sec.IV-C also illustrate that our method evaluated without PTs yields a relatively higher CMC@1. Next, we will introduce details of the key components of our PMLH, i.e., the Multi-Scale Attention module, Part Transfer on MT-PT pairs and Re-ID loss functions for our method.

Multi-scale Attention Module: Fig.1(b) illustrates that vehicle components often exhibit large variations in shape, position and scale. Directly using bottom-to-up single-scale convolution and pooling tends to be ineffective in handling these complex variations. Particularly, as the number of layers

increases, some small visual regions will be easily missed in top layers. Therefore, to give an additional soft pixel-level attention refinement within each salient vehicle part localized by the former hard attention-based PANet, our PMNet constructs a Multi-scale Attention Module (MAM) to handle such scale variation and learn subtle yet distinguished details.

As is depicted in the yellow block in Fig.5, MAM transforms the input feature into a spatial attention mask, mask_{SA} , and a channel attention mask, mask_{CA} , respectively from a Spatial Attention Block and a Channel Attention block. Afterwards, these two masks are multiplied together to get a new attention mask, mask_{MAM} . We apply this multi-scale attention mask to the original feature f and the formula can be computed as,

$$\text{MAM}(f) = \text{mask}_{\text{SA}} \times \text{mask}_{\text{CA}} \times f + f \quad (2)$$

In the Spatial Attention Block, to make local regions uniform, we first feed feature f into three 3×3 convolutional (Conv) layers with multiple dilation ratios (1, 2 and 3) and then concatenate the output features. The concatenated feature containing multi-scale information is fed into another 3 Conv blocks to learn spatial attention. In the Channel Attention Block, f is fed into two branches respectively beginning with: Global Average Pooling (GAP) and Global Max Pooling (GMP). Then the two output features are fed into two fully connected layers and added together to gain the mask_{CA} . A Sigmoid function is applied at the end of the Spatial Attention Block and Channel Attention Block to normalize the attention masks.

Note that the self-attention in PANet and the MAM in PMNet make up a combination of hard part-level and soft pixel-level attention. Such a two-stage attention method leverages the second stage module to further refine the first stage results and conducts a coarse-to-fine multi-grained search in vehicle Re-ID compared with common one-stage attention methods [35], [19].

Feature Alignment via Part Transfer: Our PMLH leverages each PT, the noisy teacher, to mentor the learning of its correspondent student, MT, so that they can both select and combine the part-relevant channels via the introduction of inductive bias. This means that built on the same backbone, PTs learn the part-specific information to construct the part-level representations for fine-grained classification and transfer their concept to MTs via hard parameter sharing of MAM as well as a Part Transfer loss.

The Part Transfer loss is demonstrated in the orange area of Task₄ in Fig.5. We firstly concatenate the K features from the K MTs and PTs to make up feature g and h , respectively. Then after normalizing g and h of each sample, we compute the mean distances between them in a batch and penalize those beyond our pre-defined margin, γ . The formula can be written as,

$$\mathcal{L}_{\text{PT}} = \max \left\{ \frac{1}{B} \left[\sum_{i=1}^B \|\mathcal{N}(g_i) - \mathcal{N}(h_i)\|_2 \right] - \gamma, 0 \right\}, \quad (3)$$

where $\mathcal{N}(\cdot)$ indicates the normalization function and B is the number of samples in a batch. g_i and h_i respectively denote

the concatenated feature g and h for the i -th sample. In our experiments, we set γ as 0.05. This loss encourages Main Tasks and Partial Tasks to pull each other closer within the γ distance, which makes sure that guided by local information of Partial Tasks, each Main Task focuses on the specific vehicle part.

C. Multi-task Learning for Vehicle Re-ID

As is depicted in the orange areas in Fig.5, our model divides this Re-ID issue into 4 sub-tasks, Task _{j} , $j \in [1, 4]$ under a shared backbone. These four sub-tasks are respectively global feature learning, ID classification sub-task for global feature, ID classification sub-task for part features and part transfer sub-task. Except for global feature learning, the rest three are contained within the Part-Mentored Learning Head. By sharing experience with each other, these four sub-tasks improve model generalization and the joint representation gives a good solution to the viewpoint variations as well as near-identical problem. .

Task₁: the global feature learning sub-task is supervised by one Cross Entropy loss and one Triplet loss [40] on its output global feature, f_g . For the following sub-tasks, we combine both feature summation and feature concatenation in our feature alignment to enable effective feature re-usage and re-exploration [42]. Task₂ and Task₃ are two ID classification sub-tasks, the K features from the classification layer of MTs, f_M^i , $i \in [1, K]$, and PTs, f_P^i , $i \in [1, K]$, are respectively summed up to get the final classification features, f_M and f_P . The formula can be written as,

$$f_M = \sum_{i=1}^K f_M^i, \quad f_P = \sum_{i=1}^K f_P^i \quad (4)$$

Cross Entropy loss is adopted on f_M and f_P in Task₂ and Task₃, respectively. As regards Task₄, it consists of the Part Transfer loss, \mathcal{L}_{PT} , two Cross Entropy losses on the concatenated features, g and h , and two Triplet losses on g and h .

In terms of loss functions, there are five ID classification losses respectively on f_g , f_M , f_P , g and h , which can be linearly summed up with 5 weights, α_j , $j \in [1, 5]$. The formula can be written as,

$$\mathcal{J}_{\text{ID}} = \sum_{j=1}^5 [\alpha_j \mathcal{L}^j(\hat{y}^j, y^j)], \quad (5)$$

where $\mathcal{L}^j(\cdot)$ denotes the Cross Entropy loss on the j -th classification score and α_j indicates the weight for the j -th ID loss. \hat{y}_i^j and y_i^j are respectively the predicted classification score and target label of the i -th training sample for the j -th ID loss.

Obviously in Equation (5), it is also essential to carefully select the weighting of each ID loss, α_j , for jointly balanced learning of all the five ID losses under a common backbone. Hence, instead of using a naïve linear sum of multiple objective losses, we leverage Homoscedastic Uncertainty Learning (HUL) [14] to automatically learn the optimal weights without extra grid search. HUL introduces a noise parameter σ_j for

each variable \hat{y}^j . As the noise σ_j increases, the loss weight, α_j , for its respective objective decreases. Assume the classification likelihood is adapted to squash a scaled version of the model output through a softmax function with a positive scalar σ_j :

$$p(\hat{y}^j | \mathbf{f}^{\mathbf{W}^j}(\mathbf{x}), \sigma_j) = \text{Softmax}\left(\frac{1}{\sigma_j^2} \mathbf{f}^{\mathbf{W}^j}(\mathbf{x})\right) \quad (6)$$

Hence, the minimization objective of this HUL-based multi-task ID loss, i.e., Equation (5), can be converted to,

$$\mathcal{J}_{\text{ID}} \approx \sum_{j=1}^5 \frac{1}{\sigma_j^2} \mathcal{L}^j(\hat{y}^j, y^j) + \sum_{j=1}^5 \log \sigma_j \quad (7)$$

In total, the five ID losses, our sample-wise Part Transfer loss, and Triplet loss [40] are combined to supervise our multi-task learning during training. Hence, the overall objective, \mathcal{J} , can be formulated as,

$$\mathcal{J} = \mathcal{J}_{\text{ID}} + \mathcal{L}_{\text{PT}} + \mathcal{L}_{\text{Triplet}}. \quad (8)$$

IV. EXPERIMENTS

In this section, we first introduce the two widely utilized vehicle Re-ID datasets and evaluation metrics. Then, we detail the implementation of the training and inference of our method. Finally, we compare our method with the state-of-the-arts and conduct ablation studies to validate the effectiveness of each component.

A. Datasets and Evaluation Metrics

1) *Datasets*: We use the two datasets below to evaluate the performance of our method.

VeRi776 [3] consists of around 51,035 bounding boxes of 776 vehicles, including 576 identities in the training set and 200 in the test set. The standard probe and gallery set respectively contain 1,678 and 11,579 images. Images in this dataset are collected by 20 cameras across block regions under different viewpoints, making it one of the most challenging Re-ID datasets. Additionally, it also provides other vehicle information, including model, color and trajectory clues.

VehicleID [15] contains totally 221,763 images for about 26,267 vehicles. The test set is divided into three sizes (small, medium and large). During inference, for each vehicle identity, one image is randomly selected as the gallery image while the others are regarded as query set. Images of this dataset are either captured under front or rear view.

2) *Evaluation Metrics*: We evaluate the model accuracy with two types of metrics in Re-ID: mean Average Precision (mAP) and Cumulative Matching Characteristics (CMC). In specific, mAP calculates the averaged area under the Precision-Recall curve (AP) for all the query images. CMC@1, 5 respectively measures the probability to locate at least one true positive in the top-1, 5 ranks.

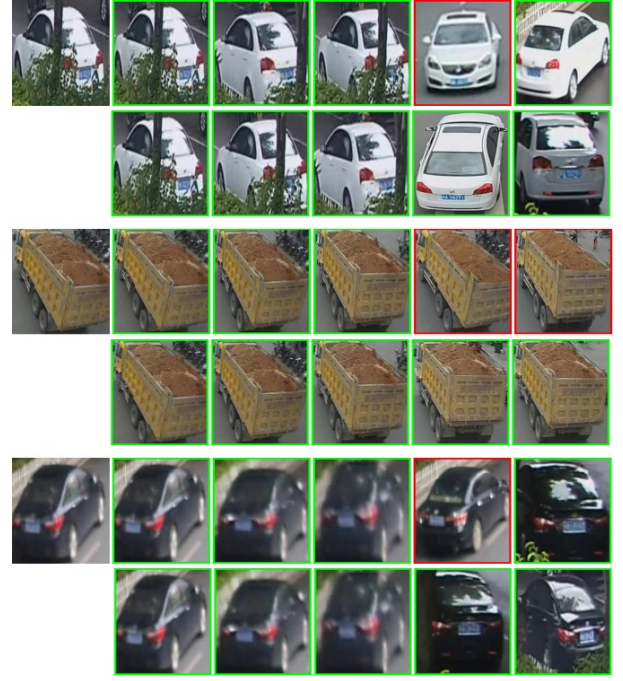


Fig. 7. Visualization of vehicle Re-ID ranking list on VeRi776. The images on the first column are the query images and the rest show retrieved gallery images. For each query sample, the first and second row respectively shows the top-5 results by baseline and PMANet. The correct and false matched vehicle images are enclosed in green and red rectangles, respectively.

B. Implementation Details

1) *Training*: Implemented with PyTorch, our model is based on the well-known Bag-of-Tricks Re-ID baseline¹ [37]. We train PANet for 100 epochs on VeRi776. The batch size is 64 and the learning rate is 1×10^{-4} . In our PMNet, we randomly sample P identities and Q images per vehicle to constitute a training batch. Finally, the batch size, B , is computed as $B = P \times Q$. Here, we set $P = 4$, $Q = 8$, $B = 32$. It should also be noted that the base learning rate of PMNet is 1.5×10^{-4} with warm-up strategy and images are resized to 256×256 . For data augmentation, we apply Random Erasing Augmentation and random horizontal flip with a probability of 0.5. As regards other hyper-parameters, in our experiments, the number of vehicle parts localized by PANet, K , is set as 3; the margin for Triplet loss [40], β , is set as 0.7. In addition, we use Adam as the optimizer.

Since there is no special dataset for occluded vehicle Re-ID, we simulate the occlusion by using a simple data augmentation technique with a probability of 0.3. For each training batch, we first randomly select an area as the obstruction region. These areas are then filled with random color patches.

2) *Inference*: To evaluate our method, we obtain g , h and global feature, f_g respectively after the BNNeck layers of our PMLH and global feature learning head. Then we calculate the Cosine Distances, D_g , D_h and D_{f_g} . Final distance between a probe and gallery set is computed as $\lambda_1 D_{f_g} + \lambda_2 D_g + \lambda_3 D_h$, where λ_i , $i \in [1, 3]$ denotes the optimal weights learned by HUL. For instance, in our experiment of evaluating PMANet

¹https://github.com/DTennant/reid_baseline_with_syncbn

TABLE I

PERFORMANCE (%) COMPARISONS WITH THE STATE-OF-THE-ARTS ON VERI776. EA IS SHORT FOR EXTRA ANNOTATION LABELED BY HUMANS.

Method	Size	EA	mAP	CMC@1	CMC@5
SPAN[8]	256x256	Y	68.9	94.0	97.6
PRReID[2]	256x256	Y	70.2	92.2	97.9
MVAN[19]	256x256	Y	72.5	92.6	97.9
CFVMNet[11]	256x256	Y	77.1	95.3	98.4
PVEN[1]	256x256	Y	79.5	95.6	98.4
RAM[5]	224x224	N	61.5	88.6	94
SAN[6]	256x256	N	72.5	93.3	97.1
SAVER[43]	256x256	N	79.6	96.4	98.6
Baseline[37]	256x256	N	77.2	95.7	97.9
Our PMANet ^o	256x256	N	81.7	96.7	98.6
Our PMANet	256x256	N	81.8	96.4	98.6
CFVMNet[11]+RR	256x256	Y	81.5	94.8	96.6
Our PMANet+RR	256x256	N	89.8	97.3	98.2

TABLE II

PERFORMANCE (%) COMPARISONS WITH THE STATE-OF-THE-ARTS ON VEHICLEID. EA IS SHORT FOR EXTRA ANNOTATION LABELED BY HUMANS. THE INPUT SIZE OF EACH METHOD IS SET TO 256×256 EXCEPT FOR RAM [5] WITH 224×224 . THE EVALUATION METRIC IS CMC.

Method	EA	Small		Medium		Large	
		@1	@5	@1	@5	@1	@5
TAMR[7]	Y	66.0	79.7	62.9	76.8	59.7	73.9
MVAN[19]	Y	-	-	-	-	72.6	83.1
PRReID[2]	Y	78.4	92.6	75.0	88.3	74.2	86.4
CFVMNet[11]	Y	81.4	94.1	77.3	90.4	74.7	88.7
PVEN[1]	Y	84.7	97.0	80.6	94.5	77.8	92.0
RAM[5]	N	75.2	91.5	72.3	87.0	67.7	84.5
SAN[6]	N	79.7	94.3	78.4	91.3	75.6	88.3
SAVER[43]	N	79.9	95.2	77.6	91.1	75.3	88.3
Our PMANet ^o	N	85.0	97.5	79.8	94.1	76.9	91.6
Our PMANet	N	85.3	97.4	79.8	94.0	76.7	91.7

on VeRi776, $\lambda_1 = 5.33$, $\lambda_2 = 4.43$, $\lambda_3 = 4.25$. In our PMANet^o in Table.I and Table.II, the Partial Tasks (PTs) are removed during evaluation, which means that λ_3 is set to 0.

C. Comparison with the State-of-the-Arts

We first compare the performance of our PMANet with a variety of recent approaches on VeRi776 [3] and VehicleID [15]. Results are respectively tabulated in Table.I and II, where EA is short for extra annotation manually labeled.

1) *Experiments on VeRi776*: We adopt CMC@1, CMC@5 and mAP as the evaluation protocol on VeRi776. As Table.I shows, in terms of whether using extra annotations, existing local-based vision methods can be divided into two categories. [2], [8], [1], [19], [11] rely on expensive key-point labels or part annotations, while [5], [6], [43] are trained without extra manual labels. [5], [6], [11] also incorporate other vehicle attributes (e.g., vehicle model, color) to enhance feature expressions. Among the EA-based works [2], [8], [1], [19], [11], PVEN [1] performs best in all the three metrics while SAVER [43] achieves relatively high results in the Non-EA category. The results in Table.I demonstrate that our PMANet sets a new state-of-the-art, surpassing PVEN and SAVER respectively by 2.3%, 2.2% in mAP. Besides, by removing PTs during inference, PMANet^o yields an even higher CMC@1. In our PMANet+RR version, we adopt [16], the re-ranking

TABLE III

ABLATION STUDIES ABOUT EACH COMPONENT OF OUR PMANET ON VERI776. ✓ IN EACH ROW DENOTES THE MODULES THAT ARE INCLUDED IN THIS EXPERIMENT. EXP-7 DENOTES OUR ENTIRE METHOD, PMANET.

Experiment Number	Global Feature Learning head	PANet	PMLH	MAM	mAP	CMC@1	CMC@5
Exp-1	✓				72.4	94.6	97.2
Exp-2	✓	✓	\mathcal{R}_2		78.5	95.7	98.0
Exp-3	✓	✓	✓		79.5	96.4	98.1
Exp-4	✓	\mathcal{R}_1	✓	✓	79.9	96.4	98.3
Exp-5		✓	✓	✓	78.1	95.3	97.8
Exp-6	✓	✓	\mathcal{R}_2	✓	78.2	95.6	98.0
Exp-7	✓	✓	✓	✓	81.8	96.4	98.6

method, as a Re-ID post-processing technique. As a result, we can observe that the mAP greatly rises to 89.8% and the CMC@1 increases to 97.3%. Fig.7 demonstrates some sample vehicle Re-ID results on VeRi776. Compared with the retrieved ranking list of the baseline, it is clear that our method produces more reliable results. These top-5 results show that our method is more robust to viewpoint variation, low resolution, background clutter and is also more capable of mining fine-grained local clues to distinguish near-identical vehicles.

2) *Experiments on VehicleID*: Since there is only one ground-truth for each query vehicle in VehicleID, merely CMC@1 and CMC@5 are compared in this dataset. Table.II illustrates the comparison results on the small, medium, and large test sets. Depending on the usage of extra annotation, Table.II groups existing methods into two categories. Results show that our proposed PMANet beats all the models in the Non-EA category, with an average improvement of 2.6% in CMC@1 and 2.8% in CMC@5. In the EA-based category, with an increase of 0.6% in CMC@1 and 0.4% in CMC@5, our method performs best on the small test set. As for the medium and large test sets, our method produces the second-best CMC@1 and CMC@5. Although our results are slightly lower than those of PVEN [1] on the medium and large test set, our method saves the cost for dense key-point labels required by PVEN. Our approach is more suitable for practical applications.

D. Ablation Study

1) *Component Analysis*: In this section, we conduct comparative experiments to validate the effectiveness of the proposed components, including Global Feature Learning Head (GFLH), Part Attention Network (PANet), Part-Mentored Learning Head (PMLH) and Multi-scale Attention Module (MAM). Detailed results are tabulated in Table.III and all the experiments are evaluated with Partial Tasks. In Table.III, \mathcal{R}_1 indicates that in Exp-4, PANet is replaced by Uniform Division for part mask generation and \mathcal{R}_2 denotes that PMLH is replaced by K single branches with plain convolution layers for local feature learning.

Global Feature Learning Head. By comparing Exp-5 and Exp-7, we can observe a dramatic increase of 3.7%, 1.1% and 0.6% in mAP, CMC@1 and CMC@5, respectively. This

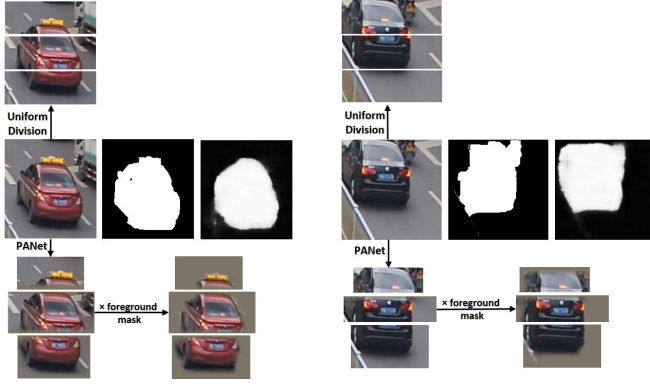


Fig. 8. Examples of generated masks by Uniform Division and our PANet. The sub-figure on the first row illustrate three parts vertically split by Uniform Division. The three figures on the second row respectively represent the sample image, the coarse foreground mask by GrabCut [36] and the refined one by our PANet. On the third row, the two sub-figures exhibit the K different part masks predicted by PANet and these K part masks multiplied with the refined foreground mask.

validates the effectiveness of our Global Feature Learning Head and shows that this global head and PMLH provide complementary information for each other.

Part Attention Network. Since PMLH requires K prior partial masks to conduct part-mentored feature aggregation, we replace PANet with a simple Uniform Division for mask generation in Exp-4. Uniform Division, which evenly splits the feature map into K stripes, is a common way utilized in [5], [6]. As is tabulated in Table.III, PMANet beats Exp-4 by 1.9% in mAP and 0.3% in CMC@5. Moreover, such a naive splitting strategy is unstable. As Fig.8 depicts, especially when a car body is unevenly distributed in the image, Uniform Division suffers from spatial misalignment and might miss some crucial information. In contrast, our PANet is able to locate different salient vehicle parts (e.g., vehicle roof, windscreen, lights) with almost all the subtle cues, such as personalized decorations and inspection marks. It is also robust to background clutter and noises.

Part-Mentored Learning Head. Instead of using part-guided learning structure, Exp-2 and Exp-6 replace PMLH with K plain convolutional branches respectively with and without MAM for detailed local feature extraction. Comparing Exp-6 with Exp-7, PMLH boosts the performance by 3.6% in mAP and 0.8% in CMC@1. Comparing Exp-2 with Exp-7, our PMANet also leads to an increase of 3.3% in mAP and 0.7% in CMC@1. These two comparisons prove that our part transfer manner shows a superior capability of extracting part-level clues than plain convolution branches.

Multi-scale Attention Module. The next contribution needing to be investigated is our soft attention, Multi-scale Attention Module (MAM). PANet automatically localizes informative regions but treats pixels within each salient part equally. Afterwards, MAM performs a second closer look at these parts for pixel-wise local feature enhancement to decrease inter-class similarity. Comparing Exp-7 with Exp-3, MAM brings an improvement of 2.3% in mAP and 0.5% in CMC@5. Furthermore, we visualize response maps on K branches of PMLH to explore how our MAM affects feature learning

TABLE IV
COMPARISON EXPERIMENTS TO VALIDATE MULTI-SCALE ATTENTION MODULE (MAM) ON VERI776. FOR THE FIRST AND SECOND ROW, MAM IN PMNET IS REPLACED BY SE-NET [34] AND RESIDUAL ATTENTION MODULE ADAPTED IN [7]

Method	mAP	CMC@1	CMC@5
PANet+SE-Net	81.0	96.8	98.2
PANet+Residual Attention Module	80.7	96.7	98.7
PMANet	81.8	96.4	98.6

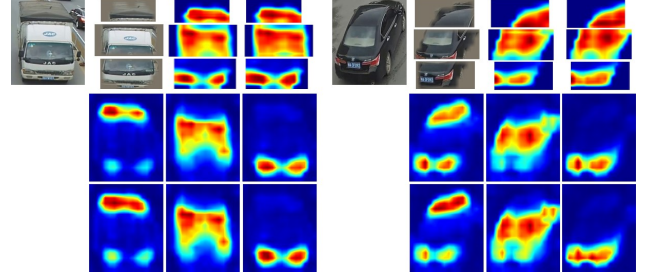


Fig. 9. Examples of response maps. the first row of each sub-figure respectively shows the original image, K part masks by PANet, response maps of K Partial Tasks before MAM, and response maps of K Partial Tasks after MAM. The second and the third row of each sub-figure show each response map of the K Main Tasks before and after MAM, respectively.

and the visualized maps are shown in Fig.9. By comparing response maps before and after the MAM in each Main Task as well as Partial Task, we can observe that the MAM assists in capturing and amplifying more subtle clues. In addition, we also compare MAM with other attention methods to verify its superiority. Among existing approaches in vehicle ReID, SE-Net [34] is a channel-wise attention commonly utilized in vision models; TAMR [7] leverages Residual Attention Module in its regional feature learning. Therefore, we replace MAM with these two attention modules on the second and third row of Table.IV. Clearly, mAP drops by 0.8% and 1.1%, respectively. Therefore, compared with SE-Net and Residual Attention Module employed in TAMR [7], our MAM exhibits better ability in handling complex scale variation and mining multi-grained clues.

2) *Validation of Part Transfer*: Instead of learning features with plain Conv layers in a single branch [7], [8], [1], our Part-Mentored learning Head (PMLH) introduces K Main-Partial Task pairs and leverages hard parameter sharing along with a sample-wise Part Transfer loss to convey part information from Partial Tasks (PT) to Main Tasks (MT). Part transfer aims to align the feature space of each MT-PT pair. As is described

TABLE V
EXPERIMENTS TO VALIDATE THE EFFECTIVENESS OF PART TRANSFER, WHICH IS REALIZED VIA PARAMETER SHARING AND OUR PART TRANSFER LOSS, \mathcal{L}_{PT} , ON VERI776. *w/o* DENOTES WITHOUT.

Method	mAP	CMC@1	CMC@5
w/o parameter sharing	81.1	96.3	98.4
w/o \mathcal{L}_{PT}	80.2	96.7	98.6
w/o parameter sharing & \mathcal{L}_{PT}	80.6	96.4	98.3
PMANet	81.8	96.4	98.6

TABLE VI
EXPERIMENTS TO VERIFY THE SUPERIORITY OF OUR MULTI-TASK
LEARNING WITH FOUR SUB-TASKS AND COMBINATION OF FEATURE
SUMMATION & CONCATENATION ON VERI776.

Method	mAP	CMC@1	CMC@5
w/o classification tasks	78.4	95.7	97.9
w/o part transfer task	79.1	95.6	98.1
w/o feature summation	79.8	96.3	98.2
w/o feature concatenation	80.6	96.0	98.2
PMANet	81.8	96.4	98.6

TABLE VII
EXPERIMENTS TO INVESTIGATE HOMOSCEDASTIC UNCERTAINTY
LEARNING ON VERI776. *WR* DENOTES WEIGHTING RATIO.

Method	mAP	CMC@1	CMC@5
w/o HUL	80.5	96.5	98.0
(<i>WR</i> :1:1:1:1:1)			
w/o HUL	80.4	96.2	98.7
(<i>WR</i> :2:1:1:1:1)			
w/o HUL	79.8	96.4	98.0
(<i>WR</i> :4:1:1:1:1)			
Add HUL	80.7	96.1	98.1
from Epoch30			
PMANet	81.8	96.4	98.6

in Sec.IV-D1, PMLH exhibits a superior local feature learning ability compared with using plain convolutional branches.

Moreover, Fig.9 shows visualized response maps of PTs and MTs in each branch. Apparently, response maps of each MT-PT pair mainly concentrate on the same vehicle part, and the K branches concentrate on K different regions which are located by PANet. This means that realized by parameter sharing and the novel Part Transfer loss, part transfer successfully guides the learning of MTs with concept conveyed in PTs. Next, we conduct experiments to verify the function of parameter sharing and our Part Transfer loss, \mathcal{L}_{PT} , in Table.V. With a respective increase of 1.6%, 0.7% in mAP, \mathcal{L}_{PT} and parameter sharing prove to be beneficial.

3) *Validation of Our Loss Functions*: In this sub-section, we respectively present our experiments to investigate multi-task learning with Homoscedastic Uncertainty Learning and our combination of feature summation as well as concatenation.

Multi-task Learning with Homoscedastic Uncertainty Learning. In our paper, we model this Re-ID issue as 4 sub-tasks. With the shared backbone, these 4 different tasks can be trained end-to-end in our unified feature learning network, PMNet, and achieve the optimal model generalization with the help of Homoscedastic Uncertainty Learning (HUL). Here we first validate the effectiveness of our multi-task learning idea in Table.VI and then investigate the superiority of adopting HUL in Table.VII on Veri776. All the experiments are evaluated with PTs. In Table.VI, *w/o* classification tasks means to remove the identity classification sub-task for global features and identity classification sub-task for part features while the second row denotes an experiment without the part transfer sub-task. In comparison with results on the first two rows in Table.VI, PMANet performs best. In detail, compared with the first row, our PMANet increases the mAP, CMC@1 by

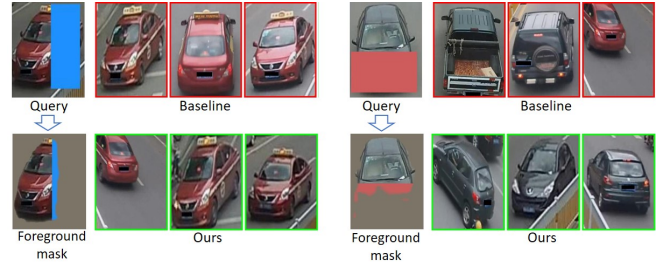


Fig. 10. Visualization results on occluded test set by [30]. In each sub-figure, images on the first column exhibit the query and the foreground mask generated by the first step of PMANet. Images on the second column show the top-3 retrieval results of the baseline and our method. **Green** and **red** rectangles indicate correct and wrong results, respectively.

3.4% and 0.7%. In comparison with results on the second row, it is observed that our part transfer sub-task boosts the mAP by 2.7%. This demonstrates that our 4 different sub-tasks provide complementary information for each other, which helps increase inter-instance variance and thus facilitate our final fine-grained re-identification task for vehicles, especially for near-duplicated identities.

For the first three rows in Table.VII, we remove HUL and manually select three different weights. In the fourth row, we incorporate HUL at training epoch 30 to relieve the influence of model noises on weight learning at the beginning of training. This is because the model is quite unstable and sensitive to noises at the beginning of training, thus making the noise parameters introduced by HUL, σ_j , increase rapidly. Since the ID loss weights are inversely proportional to the noise parameters, they will decline with the increase of σ_j , making it hard for the model to converge. Apart from speeding the convergence process during training, results in Table.VII illustrate that HUL helps save the time cost by extra manual tuning and is robust to hyper-parameter changes.

Combination of Feature Summation and Concatenation. As regards feature alignment, we incorporate feature summation with concatenation to enable both feature re-usage and re-exploration. Statistics in the third and fourth row in Table.VI show that our combined alignment structure achieves the optimal result in terms of mAP, CMC@1 and CMC@5. It is also observed that our model merely with feature concatenation is more effective than that merely with feature summation, yielding a 0.8% increase at mAP.

E. Occluded Vehicle Re-ID

To validate the robustness to occlusion, we firstly show some visualization results of the baseline and our PMANet in Fig.10. We can observe that the baseline often wrongly regards the occlusion color as the texture of the query image, while the foreground masks generated by PANet successfully avoid simulated occlusion color blocks. Therefore, our method effectively achieves robustness to viewpoint variation under occluded scenarios. To give a fair comparison, we compare our method with the baseline and the state-of-art ASAN [30] on the small test set designed by [30], as shown in Table.VIII. This small test set totally includes 60 identities and 600

TABLE VIII

COMPARISON EXPERIMENTS IN OCCLUDED VEHICLE RE-ID. FOR THE SMALL TEST SET, WE USE THE SAME TEST SET DESIGNED BY [30]. WITH 1678 IDENTITIES FOR QUERY, THE LARGE TEST SET IS CONSTRUCTED BASED ON THE TEST SET OF VERI776 [3]

Method	Small			Large		
	mAP	CMC@1	CMC@5	mAP	CMC@1	CMC@5
ASAN[30]	53.3	68.8	90.1	-	-	-
Baseline	60.1	70.7	90.7	54.5	75.9	85.8
PMANet	85.3	96.0	99.7	65.7	85.3	91.6
PMANet ^o	85.7	96.0	99.7	66.2	86.0	91.8

images, with 300 for query and 300 for gallery. Our PMANet surpasses the others with a significant improvement of over 25% in both mAP and CMC@1 on this small test set. Besides, we construct a large test set by applying random color patches to the query set of VeRi776 as shown in Fig.10. This large test set contains 200 identities and 11579 images, with 1678 for query and the rest of the images for gallery. Compared with the baseline, our method still performs best by over 10% in mAP, verifying the generalization of our model.

V. CONCLUSION

In this paper, we propose a Part-Mentored Attention Network (PMANet) consisting of two steps, a weakly-supervised Part Attention Network (PANet) for vehicle part localization and a Part-Mentored Network (PMNet) for feature aggregation. Mimicking human object recognition strategy, these two steps construct a two-stage attention structure and perform a coarse-to-fine search among vehicles. In PANet, the first stage attention locates informative vehicle parts under weak supervision with a part-level hard attention. Then PMNet employs a soft pixel-level attention as the second stage attention to learn more detailed multi-scale clues within each vehicle part. To address the two weaknesses of the standard single local feature learning branch structure, PMNet builds one Main task and Partial Task for each vehicle part. Each Partial Task is regarded as a noisy teacher to guide the learning of Main Task for more robust local features. This Re-ID issue is modeled as 4 sub-tasks under a shared backbone and experiments demonstrate that our method beats existing approaches with an average increase of 2.63%, 2.77% in CMC@1, CMC@5 on the large dataset, VehicleID [15], and 2.2% in mAP on the small dataset, VeRi776 [3], without any additional annotations. Moreover, results on occluded vehicle Re-ID test set show the robustness to background interference and occlusion.

REFERENCES

- [1] D. Meng, L. Li, X. Liu, Y. Li, S. Yang, Z.-J. Zha, X. Gao, S. Wang, and Q. Huang, "Parsing-based view-aware embedding network for vehicle re-identification," in *Proceedings of the IEEE/CVF Conference on Computer Vision and Pattern Recognition*, 2020, pp. 7103–7112.
- [2] B. He, J. Li, Y. Zhao, and Y. Tian, "Part-regularized near-duplicate vehicle re-identification," in *Proceedings of the IEEE/CVF Conference on Computer Vision and Pattern Recognition*, 2019, pp. 3997–4005.
- [3] X. Liu, W. Liu, T. Mei, and H. Ma, "Provid: Progressive and multi-modal vehicle reidentification for large-scale urban surveillance," *IEEE Transactions on Multimedia*, vol. 20, no. 3, pp. 645–658, 2017.
- [4] Y. Shen, T. Xiao, H. Li, S. Yi, and X. Wang, "Learning deep neural networks for vehicle re-id with visual-spatio-temporal path proposals," in *Proceedings of the IEEE International Conference on Computer Vision*, 2017, pp. 1900–1909.
- [5] X. Liu, S. Zhang, Q. Huang, and W. Gao, "Ram: a region-aware deep model for vehicle re-identification," in *2018 IEEE International Conference on Multimedia and Expo (ICME)*. IEEE, 2018, pp. 1–6.
- [6] J. Qian, W. Jiang, H. Luo, and H. Yu, "Stripe-based and attribute-aware network: A two-branch deep model for vehicle re-identification," *Measurement Science and Technology*, vol. 31, no. 9, p. 095401, 2020.
- [7] H. Guo, K. Zhu, M. Tang, and J. Wang, "Two-level attention network with multi-grain ranking loss for vehicle re-identification," *IEEE Transactions on Image Processing*, vol. 28, no. 9, pp. 4328–4338, 2019.
- [8] T.-S. Chen, C.-T. Liu, C.-W. Wu, and S.-Y. Chien, "Orientation-aware vehicle re-identification with semantics-guided part attention network," in *European Conference on Computer Vision*. Springer, 2020, pp. 330–346.
- [9] Y. Zhao, C. Shen, H. Wang, and S. Chen, "Structural analysis of attributes for vehicle re-identification and retrieval," *IEEE Transactions on Intelligent Transportation Systems*, vol. 21, no. 2, pp. 723–734, 2019.
- [10] X. Zhang, R. Zhang, J. Cao, D. Gong, M. You, and C. Shen, "Part-guided attention learning for vehicle instance retrieval," *IEEE Transactions on Intelligent Transportation Systems*, 2020.
- [11] Z. Sun, X. Nie, X. Xi, and Y. Yin, "Cfvmnet: A multi-branch network for vehicle re-identification based on common field of view," in *Proceedings of the 28th ACM International Conference on Multimedia*, 2020, pp. 3523–3531.
- [12] J. Redmon, S. Divvala, R. Girshick, and A. Farhadi, "You only look once: Unified, real-time object detection," in *Proceedings of the IEEE conference on computer vision and pattern recognition*, 2016, pp. 779–788.
- [13] Z. Wang, L. Tang, X. Liu, Z. Yao, S. Yi, J. Shao, J. Yan, S. Wang, H. Li, and X. Wang, "Orientation invariant feature embedding and spatial temporal regularization for vehicle re-identification," in *Proceedings of the IEEE International Conference on Computer Vision*, 2017, pp. 379–387.
- [14] A. Kendall, Y. Gal, and R. Cipolla, "Multi-task learning using uncertainty to weigh losses for scene geometry and semantics," in *Proceedings of the IEEE conference on computer vision and pattern recognition*, 2018, pp. 7482–7491.
- [15] H. Liu, Y. Tian, Y. Yang, L. Pang, and T. Huang, "Deep relative distance learning: Tell the difference between similar vehicles," in *Proceedings of the IEEE conference on computer vision and pattern recognition*, 2016, pp. 2167–2175.
- [16] Z. Zhong, L. Zheng, D. Cao, and S. Li, "Re-ranking person re-identification with k-reciprocal encoding," in *Proceedings of the IEEE Conference on Computer Vision and Pattern Recognition*, 2017, pp. 1318–1327.
- [17] S. Lian, W. Jiang, and H. Hu, "Attention-aligned network for person re-identification," *IEEE Transactions on Circuits and Systems for Video Technology*, 2020.
- [18] W. Liu, D. Anguelov, D. Erhan, C. Szegedy, S. Reed, C.-Y. Fu, and A. C. Berg, "Ssd: Single shot multibox detector," in *European conference on computer vision*. Springer, 2016, pp. 21–37.
- [19] S. Teng, S. Zhang, Q. Huang, and N. Sebe, "Multi-view spatial attention embedding for vehicle re-identification," *IEEE Transactions on Circuits and Systems for Video Technology*, vol. 31, no. 2, pp. 816–827, 2020.
- [20] M. Jaderberg, K. Simonyan, A. Zisserman, and K. Kavukcuoglu, "Spatial transformer networks," *arXiv preprint arXiv:1506.02025*, 2015.
- [21] X.-S. Wei, J.-H. Luo, J. Wu, and Z.-H. Zhou, "Selective convolutional descriptor aggregation for fine-grained image retrieval," *IEEE Transactions on Image Processing*, vol. 26, no. 6, pp. 2868–2881, 2017.
- [22] H. Yao, S. Zhang, R. Hong, Y. Zhang, C. Xu, and Q. Tian, "Deep representation learning with part loss for person re-identification," *IEEE Transactions on Image Processing*, vol. 28, no. 6, pp. 2860–2871, 2019.
- [23] Z. Zheng, L. Zheng, and Y. Yang, "Pedestrian alignment network for large-scale person re-identification," *IEEE Transactions on Circuits and Systems for Video Technology*, vol. 29, no. 10, pp. 3037–3045, 2018.
- [24] Y. Zhou and L. Shao, "Vehicle re-identification by adversarial bi-directional lstm network," in *2018 IEEE Winter Conference on Applications of Computer Vision (WACV)*. IEEE, 2018, pp. 653–662.
- [25] Y. Lou, Y. Bai, J. Liu, S. Wang, and L. Duan, "Veri-wild: A large dataset and a new method for vehicle re-identification in the wild," in *Proceedings of the IEEE/CVF Conference on Computer Vision and Pattern Recognition*, 2019, pp. 3235–3243.

- [26] Z. Zhang, C. Lan, W. Zeng, and Z. Chen, “Densely semantically aligned person re-identification,” in *Proceedings of the IEEE/CVF Conference on Computer Vision and Pattern Recognition*, 2019, pp. 667–676.
- [27] P. Ren and J. Li, “Factorized distillation: Training holistic person re-identification model by distilling an ensemble of partial reid models,” *arXiv preprint arXiv:1811.08073*, 2018.
- [28] C. Ding, K. Wang, P. Wang, and D. Tao, “Multi-task learning with coarse priors for robust part-aware person re-identification,” *IEEE Transactions on Pattern Analysis and Machine Intelligence*, 2020.
- [29] X. Lin, S. Peng, Z. Ma, X. Zhou, and A. Zheng, “Occlusion based discriminative feature mining for vehicle re-identification,” in *International Conference of Pioneering Computer Scientists, Engineers and Educators*. Springer, 2020, pp. 246–257.
- [30] H. Jin, S. Lai, and X. Qian, “Occlusion-sensitive person re-identification via attribute-based shift attention,” *IEEE Transactions on Circuits and Systems for Video Technology*, 2021.
- [31] K. Fu, D.-P. Fan, G.-P. Ji, and Q. Zhao, “Jl-dcf: Joint learning and densely-cooperative fusion framework for rgb-d salient object detection,” in *Proceedings of the IEEE/CVF conference on computer vision and pattern recognition*, 2020, pp. 3052–3062.
- [32] A. Vaswani, N. Shazeer, N. Parmar, J. Uszkoreit, L. Jones, A. N. Gomez, L. Kaiser, and I. Polosukhin, “Attention is all you need,” *arXiv preprint arXiv:1706.03762*, 2017.
- [33] J. Fu, J. Liu, H. Tian, Y. Li, Y. Bao, Z. Fang, and H. Lu, “Dual attention network for scene segmentation,” in *Proceedings of the IEEE/CVF Conference on Computer Vision and Pattern Recognition*, 2019, pp. 3146–3154.
- [34] J. Hu, L. Shen, and G. Sun, “Squeeze-and-excitation networks,” in *Proceedings of the IEEE conference on computer vision and pattern recognition*, 2018, pp. 7132–7141.
- [35] S. Teng, X. Liu, S. Zhang, and Q. Huang, “Scan: Spatial and channel attention network for vehicle re-identification,” in *Pacific Rim conference on multimedia*. Springer, 2018, pp. 350–361.
- [36] C. Rother, V. Kolmogorov, and A. Blake, ““ grabcut” interactive foreground extraction using iterated graph cuts,” *ACM transactions on graphics (TOG)*, vol. 23, no. 3, pp. 309–314, 2004.
- [37] H. Luo, Y. Gu, X. Liao, S. Lai, and W. Jiang, “Bag of tricks and a strong baseline for deep person re-identification,” in *Proceedings of the IEEE/CVF Conference on Computer Vision and Pattern Recognition Workshops*, 2019, pp. 0–0.
- [38] H. Zheng, J. Fu, Z.-J. Zha, and J. Luo, “Looking for the devil in the details: Learning trilinear attention sampling network for fine-grained image recognition,” in *Proceedings of the IEEE/CVF Conference on Computer Vision and Pattern Recognition*, 2019, pp. 5012–5021.
- [39] K. He, X. Zhang, S. Ren, and J. Sun, “Deep residual learning for image recognition,” in *Proceedings of the IEEE conference on computer vision and pattern recognition*, 2016, pp. 770–778.
- [40] A. Hermans, L. Beyer, and B. Leibe, “In defense of the triplet loss for person re-identification,” *arXiv preprint arXiv:1703.07737*, 2017.
- [41] G. Wang, Y. Yuan, X. Chen, J. Li, and X. Zhou, “Learning discriminative features with multiple granularities for person re-identification,” in *Proceedings of the 26th ACM international conference on Multimedia*, 2018, pp. 274–282.
- [42] Y. Chen, J. Li, H. Xiao, X. Jin, S. Yan, and J. Feng, “Dual path networks,” *arXiv preprint arXiv:1707.01629*, 2017.
- [43] P. Khorramshahi, N. Peri, J.-c. Chen, and R. Chellappa, “The devil is in the details: Self-supervised attention for vehicle re-identification,” in *European Conference on Computer Vision*. Springer, 2020, pp. 369–386.